Nanoscale

PAPER

View Article Online
View Journal | View Issue

Cite this: *Nanoscale*, 2018, **10**, 19125

Label free localization of nanoparticles in live cancer cells using spectroscopic microscopy†

Graham L. C. Spicer,[a] Luay Almassalha,[b] Ignacio A. Martinez,[c] Ronald Ellis,[a] John E. Chandler,[b] Scott Gladstein,[b] Di Zhang,[b] The-Quyen Nguyen,[b] Seth Feder,[b] Hariharan Subramanian,[b] Roberto de la Rica,[d] Sebastian A. Thompson*[e] and Vadim Backman*[b]

Gold nanoparticles (GNPs) have become essential tools used in nanobiotechnology due to their tunable plasmonic properties and low toxicity in biological samples. Among the available approaches for imaging GNPs internalized by cells, hyperspectral techniques stand out due to their ability to simultaneously image and perform spectral analysis of GNPs. Here, we present a study utilizing a recently introduced hyperspectral imaging technique, live-cell PWS, for the imaging, tracking, and spectral analysis of GNPs in live cancer cells. Using principal components analysis, the extracellular or intracellular localization of the GNPs can be determined without the use of exogenous labels. This technique uses wide-field white light, assuring minimal toxicity and suitable signal-to-noise ratio for spectral and temporal resolution of back-scattered signal from GNPs and local cellular structures. The application of live-cell PWS introduced here could make a great impact in nanomedicine and nanotechnology by giving new insights into GNP internalization and intracellular trafficking.

Received 13th September 2018,
Accepted 30th September 2018

DOI: 10.1039/c8nr07481j

rsc.li/nanoscale

Introduction

In the last few decades, GNPs have become widely used in a variety of biological disciplines, such as cancer treatment and diagnostics,[1,2] drug delivery,[3] and plasmonic sensors,[4] among others.[5] There are several benefits associated with the use of GNPs, including their photostability and low cellular toxicity. Furthermore, GNPs with different morphologies and sizes can easily be fabricated and functionalized with a variety of polymers and bioresponsive ligands.[6,7] This provides a flexible platform for imaging biological systems because the optical properties of the particles can be finely tuned based on the spectral needs of the experimental design. However, there are many unanswered questions about the interaction between GNPs and cells regarding GNP uptake, localization, and photoxicity.[8]

Techniques for tracking GNPs in cells, such as two-photon microscopy,[9] dark-field microscopy,[10] Optical Coherence Tomography,[11] Magnetic Resonance Imaging,[12] and many others[13] have been able to adequately image GNPs but present some limitations. Dark-field microscopy results in low phototoxicity for the cells, and is based only on the light scattered by the GNPs. However, previous studies have shown that the signal from light scattered by the cell's organelles may combine with the characteristic spectrum of light scattered by the GNPs, thus obscuring the signal from the nanoparticles.[14] The other commonly used technique, two-photon microscopy, is based on the nonlinear excitation and resulting luminescence emission from GNPs irradiated with a pulsed laser. However, the use of a high-power laser leads to phototoxicity, making two-photon microscopy unsuitable for some applications. Other imaging techniques such as optical coherence tomography or photoacoustic imaging may be used for *in vivo* imaging of GNPs in tissue by harnessing their characteristic absorption properties, but these techniques also lack the necessary spatial resolution to study intracellular localization of GNPs.[15–17]

[a]*Department of Chemical and Biological Engineering, Northwestern University, Evanston, Il 60208, USA*
[b]*Department of Biomedical Engineering, Northwestern University, Evanston, Il 60208, USA. E-mail: v-backman@northwestern.edu*
[c]*Departamento de Estructura de la Materia, Física Térmica y Electrónica and GISC, Universidad Complutense de Madrid, 28040 Madrid, Spain*
[d]*Department of Pure and Applied Chemistry, University of Strathclyde, Technology and Innovation Centre, 99 George Street, Glasgow G1 1RD, Scotland, UK*
[e]*Department of Chemistry, Hunter College, New York, NY 10065, USA. E-mail: sthompso@hunter.cuny.edu*

†Electronic supplementary information (ESI) available: ESEM images of GNP cluster surrounded by salt crystals before and after electron beam bombardment, interference image at 550 nm and quantitative colormap of RMS from HeLa cells incubated with GNPs, UV-Vis absorption spectrum of stock GNP suspension used for these studies, video GNP motion within the cell through the well-defined contrast provided in the RMS map. See DOI: 10.1039/c8nr07481j

Recent studies using hyperspectral dark-field microscopy (HDM) offer a promising alternative for studying GNPs inside cells.[14,18] The main advantage of HDM is its ability to simultaneously image and obtain scattering spectra from GNPs. Together, this information allows for the spectral identification and differentiation of light scattered by the cell's organelles and by internalized GNPs. Hyperspectral reflected light microscopy (HRLM) has also been implemented to extend the capabilities and performance of hyperspectral microscopy for 3D localization and spectral identification of GNPs in fixed cells.[14] In this study, we present the application of a new HRLM method, termed live-cell partial-wave spectroscopic (PWS) microscopy, where the spectrally-resolved interference of scattered and reflected reference signal allows for the imaging, tracking, and spectral analysis of gold nanoparticles (GNPs) in live cancer cells. Light incident upon a GNP has a characteristic spectrally-dependent probability of absorption due to plasmonic resonance, along with a characteristic scattering signal from the GNP, which is affected by this absorption spectrum and the size of the particle. PWS measures the spectrally-resolved interference between light scattered from structures within a cell and a reference signal created by the Fresnel reflection between a glass coverslip and the cell. The capability of live-cell PWS for label-free study of native nanostructure of nuclear chromatin has been demonstrated previously.[19] Here, we apply this technique to also study the response of nuclear structure to treatment of live cancer cells with GNPs. This new hyperspectral reflected light microscopy technique can address current questions regarding the relationship between the aggregation of GNPs and their uptake by cells.[20]

Experimental section

Live-cell PWS instrument

The live-cell PWS instrument is described in a previous publication. Briefly, sample illumination is a low numerical aperture beam from a high power broad-spectrum LED source (Excelitas X-Cite 120 LED). During all imaging, cells are kept in a stage top incubation chamber kept at 37 C with 5% CO_2 atmosphere. For this imaging, cells are plated and grown in glass-bottom imaging dishes with an imaging window of number 0 glass coverslip. Scattered light from the sample is collected with a high numerical aperture oil-immersion objective (63×, NA = 1.4) and passed through a liquid crystal tunable filter (LCTF) that was programmed to sweep through a wavelength range from 500–700 nm in 1 nm increments for spectrally-resolved acquisition of the interference signal.

AOTF PWS instrument

The HRLM instrument used in this experiment consisted of an automated epi-illumination widefield microscope with spectrally tunable illumination as described previously.[22] Broadband light from a Xenon lamp (66902, 100 W, Oriel Instruments, Stratford, Connecticut) was spectrally filtered by an AOTF (HSI-300, Gooch & Housego, Orlando, Florida). The spectrally filtered illumination light was then passed through an aperture stop to set the illumination numerical aperture (NA ~ 0.15) before illuminating the sample. Scattered light from the sample was collected using a high-NA objective lens (40×, NA = 0.6, LUCPlanFLN, Olympus, Center Valley, Pennsylvania). Images corresponding to each illumination wavelength, typically 500–700 nm with 1 nm steps, were acquired using a high-speed CMOS camera (Hamamatsu, ORCA-Flash 2.8, Bridgewater, New Jersey). Raw data consisted of a hyperspectral image cube $I(x,y,\lambda)$ containing spectra at each pixel in the acquired image.

Cell culture and nanoparticle treatment

HeLa cells were obtained from ATCC and were grown in Dulbecco's modified Eagle's medium supplemented with 10% Fetal Bovine Serum (FBS). Cells were maintained in a 37 °C, 5% CO_2 humidified environment. Cells were trypsinized and plated on glass imaging dishes for imaging experiments after a two-day incubation. For incubation with GNPs, media was supplemented with 100 nm diameter methyl polymer functionalized gold nanoparticles (Nanopartz #C11-100-TM-50, Nanopartz Inc., Loveland, CO, USA) at a concentration of 4×10^6 nanoparticles per mL, after which the cells were incubated for 24 hours prior to imaging. Immediately before imaging, the medium was replaced with fresh, GNP-free imaging medium through a triple-rinse procedure.

Data analysis and imaging process

Aggregated GNPs selectively reflect and scatter light at different wavelengths, creating a characteristic reflection spectrum at the far field. The locations of spectral peaks are determined by the size of the nanoparticles and other interfacial characteristics. To identify nanoparticles of various sizes, a spectral analysis can be useful. Since the locations of the peaks are unknown, images at a single wavelength will not identify all the nanoparticles. Here we propose using (root mean square) RMS as the indicator of nanoparticles. RMS is defined as the root mean square of the zero-mean intensities in the spectrum:

$$\mathrm{RMS} = \sqrt{\frac{1}{N}\sum_{i=1}^{N}\left(I(\lambda_i) - \bar{I}\right)^2}$$

where N is the number of wavelengths, I denotes the spectrum of reflection normalized by the illumination intensity, $\bar{I}$ represents the mean intensity over the wavelength band. For each pixel of interest, RMS is large when a nanoparticle of any size is present and is small when there are no nanoparticles. Although a cell without nanoparticles can also cause oscillations in backscattered spectra, the amplitude of these oscillations is much weaker than that obtained from nanoparticles.[26] Furthermore, sizes of nanoparticles (large/small) can be identified by the average reflectance. Bright Field Reflected Images (BRFI) are obtained by averaging the full

interference image along wavelength in the range between 500 and 700 nm.

Preparation of glass slides

For ESEM imaging with HRLM correlation experiments, glass slides were cleaned in piranha solution for 1 h. After rinsing with copious amounts of water, they were dried with nitrogen. The slides were then immersed in a 1% PDDA (poly(diallyldimethylammonium chloride)) solution for 30 min, rinsed with water and dried with nitrogen. A drop of the nanoparticle solution was deposited on the slides for 5 minutes. The slides were then rinsed with water and dried with nitrogen.

ESEM imaging

Spherical gold nanoparticles (GNPs) with 40 nm diameters were deposited onto glass microscope slides by suspending the particles at a concentration of 0.1 nM in an aqueous solution. In order to induce aggregation of particles, sodium chloride was introduced to the solution at a concentration of 10 mM. The solution was then pipetted onto the glass slide and allowed to air dry prior to imaging with PWS microscopy and ESEM.

For electron microscopy imaging of GNPs deposited on a glass substrate, a FEI Quanta 400 F ESEM was used in low vacuum mode. Locations of PWS images were co-localized with ESEM imaging of the same region using permanent marker to mark the surface of the glass slide in a distinctive manner for locative cross-registration.

Whereas salt crystals in the ESEM images of these slides appeared as bright cubic structures on the order of ~400 nm in the lateral dimension, these structures were not readily apparent in PWS microscopy images. However, aggregated clusters of GNPs, which appeared as light grey clusters in the SEM images, appear as bright spots in PWS micrographs (Fig. 1A and B). This indicates a higher sensitivity of PWS microscopy to the GNP clusters compared to less reflective salt crystals. When aggregation of GNPs was not induced by the introduction of salt, the GNPs were not visible in PWS images, indicating the failure of PWS to detect the presence of singular GNPs.

Results and discussion

We first investigated the capability of partial-wave spectroscopic microscopy (PWS) to image GNPs on a glass slide in order to determine its sensitivity to GNPs particle aggregation. Since GNPs inside the cells will not be present as single GNPs due to the process of endocytosis or their interaction with cytosolic proteins, we focus our studies on aggregates of GNPs rather than single GNPs. Thus, the study was focused on characterizing the signal of aggregated GNPs using PWS. In solution, aggregation of 40 nm spherical GNPs was induced by adding 10 mM NaCl, after which the particle suspension was deposited on a glass slide, rinsed and then allowed to dry, and a selected region was imaged with both PWS (AOTF instrument described elsewhere[21,22] and in Materials and methods) and

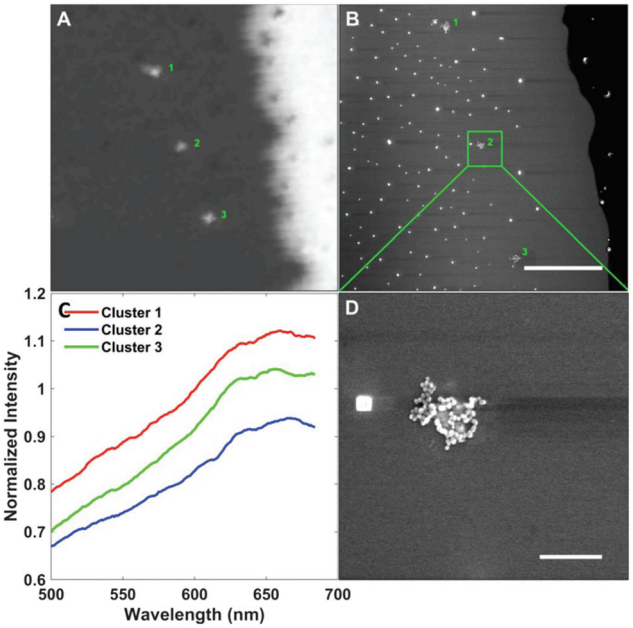

Fig. 1 (A) BFRI interference image (B) ESEM image of the same view of aggregated GNPs deposited on glass slide (scale bar = 5 μm). (C) Normalized scattering spectra from GNP clusters labeled 1, 2, and 3 measured with PWS. (D) Magnification of GNP cluster 2.

an environmental scanning electron microscope (ESEM). These co-registered images from both techniques are shown in Fig. 1. From PWS imaging, the GNPs are readily observed as bright spots in the wavelength-summed interference image (BFRI), labeled as structures 1, 2, and 3 shown in Fig. 1(a). The same structures are labeled in the ESEM image of the region shown in Fig. 1(b) where it is evident that many other bright structures corresponding to salt crystals from the carrier solution are also visible in the ESEM but not PWS images. Difference in composition of these crystal structures and GNPs was confirmed through electron beam bombardment in the ESEM, shown in ESI Fig. 1.† Furthermore, the expanded view of the region around GNP structure 2 shown in Fig. 1(d) shows that in the desiccated sample GNPs that are visible with PWS are in the form of aggregated clusters of many GNPs. Thus, for dried samples PWS is particularly sensitive to clusters of GNPs but not other, less scattering debris such as salt crystals.

PWS instrumentation

For our studies of GNPs in live cells, measurements were obtained using the live-cell PWS optical set-up shown in Fig. 2 and briefly described in Materials and methods.

PWS analysis

We applied PWS processing analysis to quantify cellular structural parameter RMS, which describes the fractal dimension of macromolecular organization in cellular compartments. In addition to quantifying this dimension, RMS also produces a highly enhanced signal contrast from GNPs in an image of the particles incubated in HeLa cells shown in Fig. 3(b), when

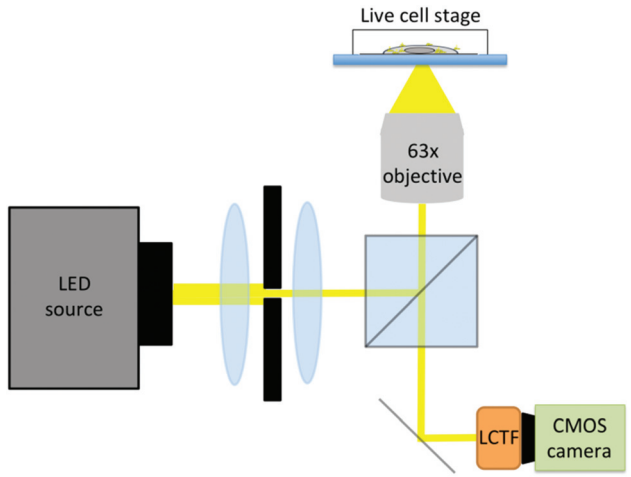

Fig. 2 Schematic of live-cell PWS instrument used for imaging experiments.

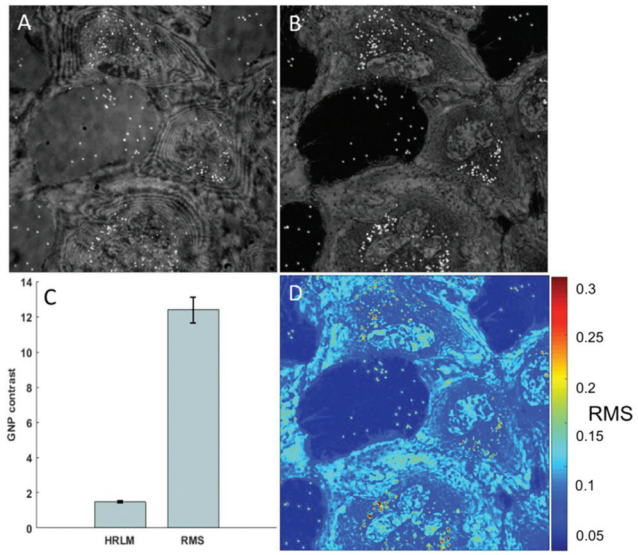

Fig. 3 Images of GNPs incubated with HeLa cells derived from (A) BFRI and (B) PWS RMS parameter. Contrast of GNPs compared with surrounding field is enhanced in RMS map compared to BFRI (C). PWS RMS map typically plotted in color scaled to magnitude of RMS value used to quantify cellular structure (D).

compared to the BFRI image, shown in Fig. 3(a). A quantitative colormap of RMS for this image is also shown in Fig. 3(d).

With live-cell PWS we were able to directly observe GNP motion within the cell through the well-defined contrast provided in the RMS map. We demonstrate the applicability of this technique allowing the label-free intra- and extra-cellular discrimination of the GNPs and the study of intra- and intercellular transport of GNPs in ESI Video S1,† where potential intercellular trafficking of a GNP can be seen from the cell on the left to the cell on the right (momentarily moving out of the focal plane between observed locations in each cell).

Principal component analysis

To determine how cellular uptake of GNPs affects their visible scattering spectra, HeLa cells were cultured under standard conditions, then incubated with 100 nm diameter spherical GNPs (Nanopartz) at a concentration of 4×10^6 particles per mL media for a period of 24 hours prior to imaging with live-cell PWS. From a single PWS image of a HeLa cell, cellular margins were manually segmented and a mask of GNP location was created using a threshold of image intensity. Averaged spectra from GNPs inside and outside of the HeLa cell, along with background intensity from cell and glass are shown in ESI Fig. 2.† It was observed that internalized GNPs had a mean spectral scattering peak shifted up in wavelength compared to GNPs outside of the cell. The mean spectral absorption of the GNP suspension used to treat the cells was independently measured using a NanoDrop UV-Vis spectrophotometer. The absorption peak of the GNP treatment suspension was centered at approximately 580 nm, and is shown in ESI Fig. 3.†

To characterize the features of the GNP scattering spectra, we performed a *K*-means clustering analysis on individual spectra from each GNP location in the PWS image. This analysis decomposes the scattering spectrum into a sum of discrete principal component functions that describe the scattering spectra from all visible GNPs in our measurements. These principal component spectra are plotted in Fig. 4(a). When we plot the mean relative contribution of each principal component to the full scattering spectrum, we can see that the full spectrum can be fairly well-characterized by the first 3 principal components, with the first component accounting for approximately 43% of the full spectral behavior of GNPs, shown in Fig. 4(b).

Overlaying the scaling factor for the first principal component in color over respective GNPs in the PWS image, it can be seen in Fig. 5 that internalized GNPs show a much higher variation in this component scaling when compared to GNPs on glass. To further show this effect, we show a plot of the first 3 principal components in Fig. 6, together which account for 69.4% of the spectral scattering shape measured from GNPs in

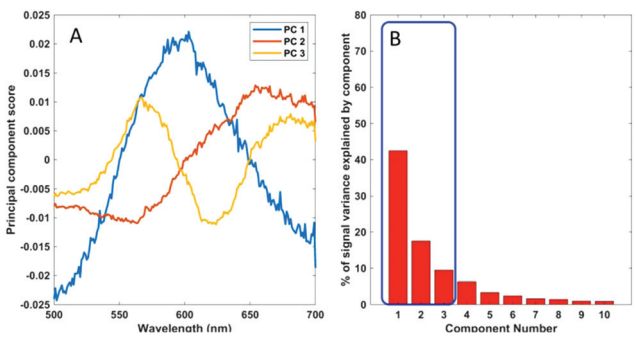

Fig. 4 Principal component spectra for the first 3 principal components of GNP scattering spectra (A). GNP scattering spectral signal explained well by the first 3 principal components, after which subsequent components each contribute less than 7% to the total spectral shape (B).

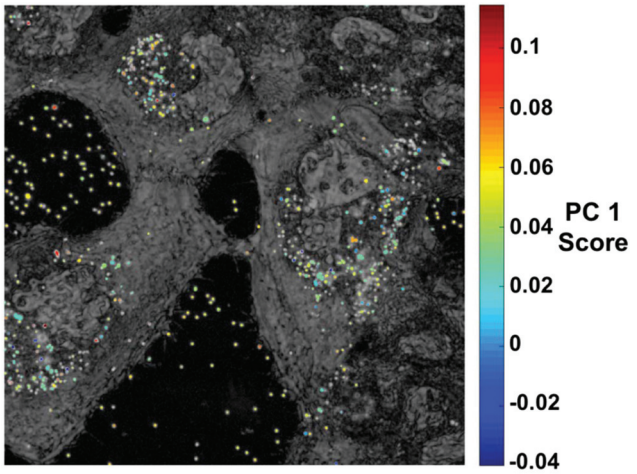

Fig. 5 Image of HeLa cells incubated with GNPs (bright specks). GNPs color-coded by score of the first spectral principal component (PC 1).

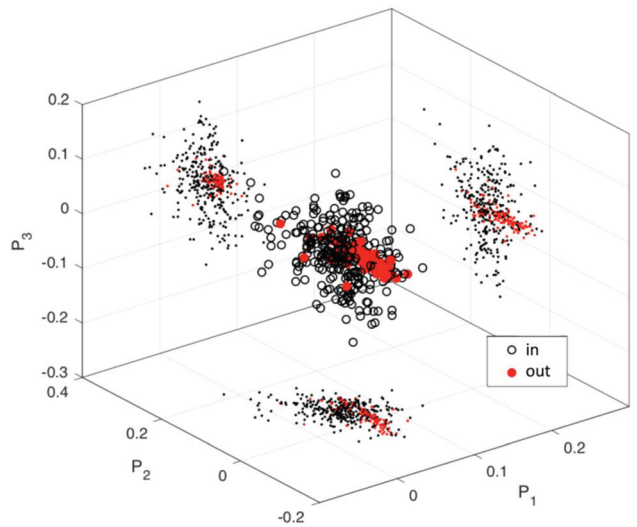

Fig. 6 3D scatter plot of principal component scores (P_1, P_2, and P_3, respectively) for each GNP location. GNPs inside cells show tighter clustering of principal component scores than GNPs outside of cells.

this experiment. Clustering of spectral character is noticeably tighter for GNPs outside of cells (scatterplot occupancy volume of 0.00049 compared to 0.0039 for internalized cells)[23] when compared to those located within cell margins, which display a very wide variation in principal component scores. These variances are potentially in concordance with the larger variety of different proteins nanoparticles interact with inside the cell compared to outside the cell.

Here, we have demonstrated the use of live-cell PWS for imaging of GNP agglomerates in live cells. When compared to a bright field reflected image (BFRI) collected by averaging backscatter image intensity across wavelength, the PWS analysis used here to obtain RMS images yields a much higher contrast of GNPs compared to the field background. This enhanced sensitivity to GNPs lends this analysis for improved imaging and segmentation of GNPs from the hyperspectral image. Furthermore, RMS has been used for quantification of cellular structure in previous work,[19,24,25] and we foresee its parallel implementation for localization and study of interactions between GNPs and live cells.

As mentioned above, live-cell PWS enables imaging of nanoparticle clusters by means of measuring the spectral signature of objects throughout the field of view. Harnessing this capability, we measured how mean scattering spectra from GNP clusters inside live HeLa cells have a higher peak wavelength than clusters outside of the cell margins.

To help understand the specific scattering spectral characteristics that might change as a consequence from this process, we performed principal component analysis on an array of all GNP cluster spectra, decomposing each into a linear sum of the characteristic component spectra. While it is unclear which biological and plasmonic modifications are directly responsible for the specific spectral features each component represents, further studies integrating controlled physicochemical changes to GNP structure and aggregation would help to clarify the individual contributions to bulk differences in spectra observed here.

An interesting observation, however, is the much larger variation in principal component scores for internalized GNPs when compared to GNPs outside the cell on the bare glass coverslip. The GNPs can clearly be identified in the cytoplasm of the HeLa cells, in agreement with the general characterization of how GNPs localize in the cytoplasm rather than the nucleus.[20] Intracellular movement of GNPs in the cytoplasm is much higher than GNPs outside of the cell, which largely remain motionless on the coverslip, as can be observed in ESI Video 1.† Measuring the spectral properties of GNPs in the cell environment will also prove valuable for photothermal applications where the light used should match the GNP plasmon, which could have changed due to aggregation or interaction with plasma proteins. By modifying the incubation protocol, different GNP populations can be imaged. For example, by incubating cells under low temperature or by inhibiting endocytosis, it will be possible to image GNP clusters on the plasma membrane. This information will allow deeper understanding of GNP–plasma membrane interactions.

Conclusions

We have presented and tested the novel application of a hyperspectral microscopy technique, live-cell PWS, for the imaging and spectral characterization of aggregated GNPs live cancer cells. This technique provides important information about the localization of the GNP clusters as well as their plasmonic properties in the cellular environment. Continued study of GNP spectra and intracellular interactions with this microscopy technique will help current research projects focused on intracellular localization and the interactions between GNPs and the plasma membrane during intracellular

uptake. We expect that this easy-to-use microscopy technique will become a useful tool in research projects pertaining to GNPs in cancer cell models.

Conflicts of interest

There are no conflicts to declare.

Acknowledgements

S. T. acknowledges a PEER/PECRE Travel Grant from WestCHEM. R. R. acknowledges a Ramon y Cajal Contract from Ministerio de Economía, Industria y Competitividad, Agencia estatal de investigacion, Universitat de les Illes Balears, Conselleria d'Innovacio, Recerca i Turisme, and the European Social Fund. IAM acknowledges funding from the Spanish Government through grants TerMic (FIS2014-52486-R) and Contract (FIS2017-83709-R) and from Juan de la Cierva-f program. GLCS acknowledges funding from NIH RO1 CA173745. This work made use of the EPIC facility of Northwestern University's NUANCE Center, which has received support from the Soft and Hybrid Nanotechnology Experimental (SHyNE) Resource (NSF ECCS-1542205), the MRSEC program (NSF DMR-1720139) at the Materials Research Center, the International Institute for Nanotechnology (IIN), the Keck Foundation, and the State of Illinois, through the IIN.

References

1 J. H. Kang, Y. Asami, M. Murata, H. Kitazaki, N. Sadanaga, E. Tokunaga, S. Shiotani, S. Okada, Y. Maehara, T. Niidome, M. Hashizume, T. Mori and Y. Katayama, *Biosens. Bioelectron.*, 2010, **25**(8), 1869–1874.
2 S. Jain, D. G. Hirst and J. M. O'Sullivan, *Br. J. Radiol.*, 2012, **85**(1010), 101–113.
3 L. Song, V. H. B. Ho, C. Chen, Z. Yang, D. Liu, R. Chen and D. Zhou, *Adv. Healthcare Mater.*, 2013, **2**, 275–280.
4 R. de la Rica and M. M. Stevens, *Nat. Nanotechnol.*, 2012, **8**(9), 1759–1764.
5 R. de La Rica and A. H. Verders, *J. Am. Chem. Soc.*, 2011, **133**, 2875–2877.
6 K. Seekell, S. Lewis, C. Wilson, S. Li, G. Grant and A. Wax, *Biomed. Opt. Express*, 2013, **4**(11), 2284–2295.
7 F. K. Alanazi, A. A. Radwan and I. A. Alsarra, *Saudi Pharm. J.*, 2010, **18**(4), 179–193.
8 H. Jiang and S. X. Sun, *Biophys. J.*, 2013, **105**(3), 609–619.
9 H. Wang, T. B. Huff, D. A. Zweifel, W. He, P. S. Low, A. Wei and J. Cheng, *Proc. Natl. Acad. Sci. U. S. A.*, 2005, **102**(44), 15752–15756.
10 M. Hu, C. Novo, A. Funston, H. Wang, H. Staleva, S. Zou, P. Mulvaney, Y. Xia and G. V. Hartland, *J. Mater. Chem.*, 2008, **18**(17), 1949–1960.
11 E. V. Zagaynova, M. V. Shirmanova, M. Y. Kirillin, B. N. Khlebtsov, A. G. Orlova, I. V. Balalaeva, M. A. Sirotkina, M. L. Bugrova, P. D. Agrba and V. A. Kamensky, *Phys. Med. Biol.*, 2008, **53**, 4995–5009.
12 P.-J. Debouttière, S. Roux, F. Vocanson, C. Billotey, O. Beuf, a. Favre-Réguillon, Y. Lin, S. Pellet-Rostaing, R. Lamartine, P. Perriat and O. Tillement, *Adv. Funct. Mater.*, 2006, **16**(18), 2330–2339.
13 R. Lahr and P. Vikesland, *ACS Sustainable Chem. Eng.*, 2014, **2**(7), 1599–1608.
14 S. Patskovsky, E. Bergeron, D. Rioux and M. Meunier, *J. Biophotonics*, 2014, **7**, 1–7.
15 O. Liba, E. D. Sorelle, D. Sen and A. De La Zerda, *Sci. Rep.*, 2016, **6**(January), 1–12.
16 J. Tucker-Schwartz and M. Skala, *SPIE Newsroom*, 2012, 2–4.
17 W. Li and X. Chen, *Nanomedicine*, 2015, **10**(2), 299–320.
18 N. Fairbairn, A. Christofidou, A. G. Kanaras, T. A. Newman and O. L. Muskens, *Phys. Chem. Chem. Phys.*, 2012, **15**(12), 4163–4168.
19 L. M. Almassalha, G. M. Bauer, J. E. Chandler, S. Gladstein, L. Cherkezyan and Y. Stypula-cyrus, *Proc. Natl. Acad. Sci. U. S. A.*, 2016, **113**(42), E6372–E6381.
20 J. C. G. Jeynes, C. Jeynes, M. J. Merchant and K. J. Kirkby, *Analyst*, 2013, **138**, 7070–7074.
21 H. Subramanian, P. Pradhan, Y. Liu, I. R. Capoglu, J. D. Rogers, H. K. Roy, R. E. Brand and V. Backman, *Opt. Lett.*, 2009, **34**(4), 518–520.
22 J. E. Chandler, C. D. Maneval, C. A. White and R. M. Levenson, *J. Biomed. Opt.*, 2013, **18**(11), 17002.
23 F. P. Preparata and S. J. Hong, *Commun. ACM*, 1977, **20**(2), 87–93.
24 G. M. Bauer, Y. Stypula-Cyrus, H. Subramanian, L. Cherkezyan, P. Viswanathan, D. Zhang, R. Iyengar, S. Bagalkar, J. Derbas, T. Graff, S. Gladstein, L. M. Almassalha, J. E. Chandler, H. K. Roy and V. Backman, *Future Sci. OA*, 2017, **3**(3), FSO206.
25 L. M. Almassalha, G. M. Bauer, W. Wu, L. Cherkezyan, D. Zhang, A. Kendra, S. Gladstein, J. E. Chandler, D. Vanderway, B. L. L. Seagle, A. Ugolkov, D. D. Billadeau, T. V. O'Halloran, A. P. Mazar, H. K. Roy, I. Szleifer, S. Shahabi and V. Backman, *Nat. Biomed. Eng.*, 2017, **1**(11), 902–913.
26 L. Cherkezyan, I. Capoglu, H. Subramanian, J. D. Rogers, D. Damania, A. Taflove and V. Backman, *Phys. Rev. Lett.*, 2013, **111**, 033903.

